Basin Research (2000) **12,** 367–380

Sediment flux from an uplifting fault block

Philip A. Allen and A. L. Densmore

Department of Geology, Trinity College, Dublin 2, Ireland
(e-mail: paallen@tcd.ie; densmora@tcd.ie)

ABSTRACT

The stratigraphy of rift basins is a direct result of sediment liberation and transport through catchment–fan systems whose dynamics are controlled by both external and internal factors. We investigate the response of catchment–fan systems established across an active normal fault to variations in both tectonic and climatic boundary conditions. Numerical experiments show that the ratio of fan area to catchment area provides a sensitive indicator of tectonic activity. A step decrease in fault slip rate results in a delayed response by the catchment–fan systems; the response time is ~ 50 kyr for a variety of parameter values. Decreased slip rate also gives rise to an abrupt but transient pulse in sediment discharge from the fans due to a drop in the hangingwall subsidence rate. In contrast, variations in climatic activity, using precipitation rate as a proxy, produce extremely rapid responses throughout the catchment–fan system. Thus, high-frequency climatic changes will overprint lower frequency tectonic variations in the stratigraphic record of fan deposits. Finally, we map out possible combinations of fault geometry, fault slip rate and precipitation rate that allow fan progradation and high rates of sediment discharge from the system.

INTRODUCTION

It is increasingly clear that an understanding of the stratigraphy of rift basins can only come through an integration of structural and thermal evolution combined with a knowledge of Earth surface processes. The way in which these different processes are linked, and the fluxes involved, is best evaluated at geological time scales by numerical modelling. Numerical landscape evolution models appropriate to rifted regions track parcels of crust through time as they are exhumed toward a surface landscape etched into a normal fault footwall. Denudation of the footwall landscape determines the spatial and temporal patterns of sediment discharge to adjacent depocentres in the fault hangingwall. The linked tectonic-erosion system therefore has characteristic length and time scales. It is particularly important to understand the sensitivity of this coupled system to changes in the tectonic and climatic boundary conditions.

Our approach is to numerically investigate the evolution and dynamics of a single uplifting fault block (Fig. 1). Tectonic displacement on the fault is essentially constant along short (~ 10 km) stretches of the range front. Transverse bedrock catchments develop on the footwall as it undergoes tectonically driven rock uplift, and deposition is primarily confined to fans adjacent to the range front. We first evaluate the effects of fault slip rate on catchment and fan areas, with reference to the well studied catchment–fan systems in the Death Valley region of the south-western USA. A series of numerical experiments then illustrate the sensitivity of catchment–fan systems to abrupt perturbations in fault slip rate and precipitation rate, as measured by variations in catchment-averaged erosion rates and fan-averaged deposition rates. We also examine the effects of these perturbations on sediment storage within the fans and on sediment discharge from the model space, both of which are key ingredients in the development of future predictive models of proximal rift basin stratigraphy.

THE NUMERICAL LANDSCAPE EVOLUTION MODEL

The landscape evolution model *Zscape* was developed by Densmore *et al.* (1998) for the specific purpose of simulating the erosional evolution of footwall mountain blocks in the Basin and Range province of the south-western USA. Details of the model were given by Densmore *et al.* (1998) and Ellis *et al.* (1999), and are summarized in Fig. 2 and Table 1. Briefly, *Zscape* is a finite-difference code that tracks both bedrock and surface elevations on a two-dimensional, square grid. The model grid measures 10×10 km, with 100-m spacing between adjacent cells. Cell positions are modified by a three-dimensional tectonic displacement field that simulates coseismic elastic deformation around a normal fault driven by a pure shear extensional strain field (Fig. 2; see discussion in Ellis *et al.*, 1999). The model faults in our experiments are straight segments, 40 km long and 15 km wide in the down-dip direction, and are embedded in an elastic half-space. Fault dip is 45° unless specified

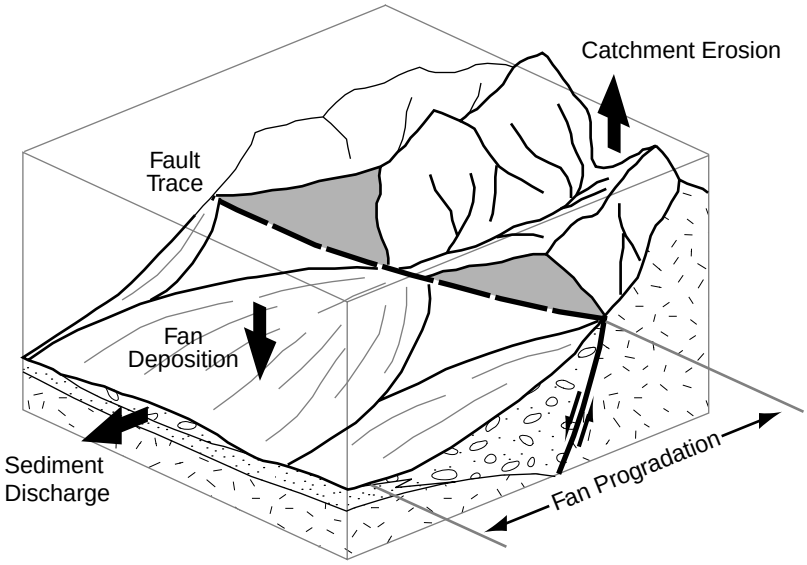

Fig. 1. Conceptual diagram of an uplifting normal fault footwall block and associated catchment–fan systems. The grey box indicates the boundaries of the model space used in our numerical experiments. Labelled arrows indicate the parameters that are tracked during evolution of the catchment–fan systems.

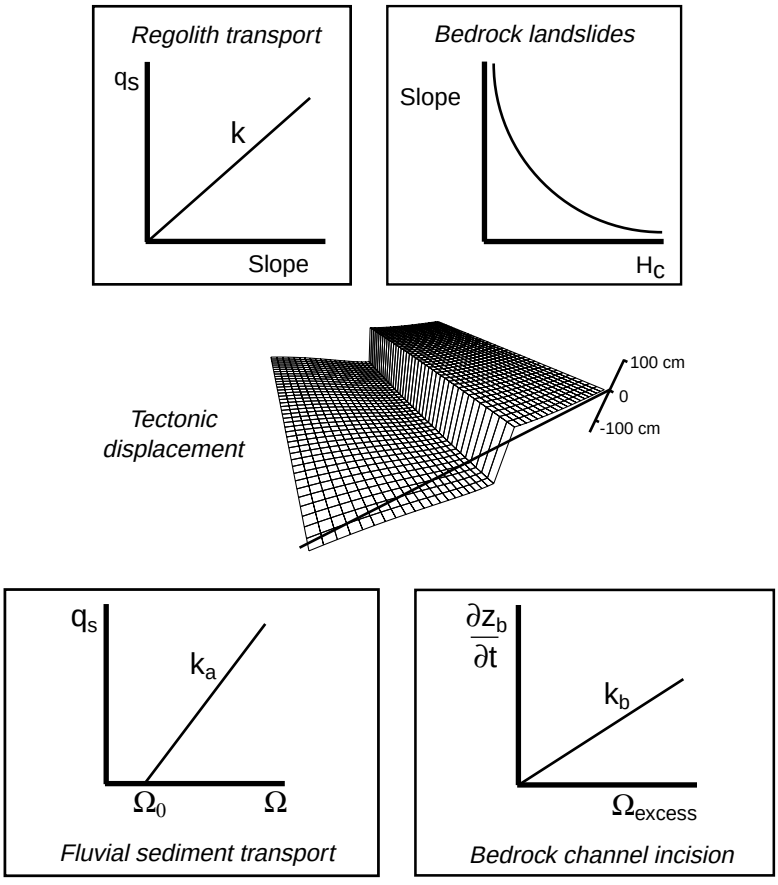

Fig. 2. Schematic diagram showing the tectonic and geomorphic algorithms that comprise the *Zscape* numerical model. The central panel shows the vertical component of the three-dimensional tectonic displacement field, which is applied to the model grid at regular intervals. Maximum footwall rock uplift during a single displacement event is 0.3 m, and maximum hangingwall subsidence is 1.4 m. Fault slip rate is dictated by the recurrence interval between displacement events; a recurrence interval of 850 yr yields a slip rate of 2.0 mm yr^{-1}. The outer panels show the geomorphic rules that act on the tectonically produced topography. The transport rate of regolith (mobile hillslope material, as distinct from bedrock), q_s, is dependent on local slope, while probability of bedrock landsliding is dependent on an inverse relationship between topographic slope and maximum stable hillslope height, H_c. Fluvial sediment transport rate, q_s, is directly proportional to stream power per unit bed width, Ω, above an empirical threshold Ω_0. Bedrock channel incision rate, $\partial z_b/\partial t$, is proportional to any excess stream power, Ω_{excess}, left over once all available sediment has been entrained. k, k_a, and k_b are constants. See Table 1 for expressions.

otherwise. To avoid edge effects and significant along-strike variations in slip rate, the 10×10-km model grid is centred on the midpoint of the fault. Long-term slip rate is variable, depending on the experiment, but in each case the strain rate across the model space is $\sim 10^{-7}\,yr^{-1}$, broadly in accord with geodetically determined strain rates across the Basin and Range (e.g. Dixon *et al.*, 1995). Importantly, model tectonic displacements are three-dimensional, so that the developing landscape is advected away from the fault via horizontal extension as well as being subject to rock uplift or subsidence.

The resulting topography is acted upon by a series of algorithms that represent the geomorphic processes of regolith transport on hillslopes, bedrock landsliding,

Table 1. Surface process algorithms used in Zscape.

Quantity	Algorithm	Variables
Rate of change of surface elevation with time, $\partial z/\partial t$	$\frac{\partial z}{\partial t}=\left(-\frac{1}{\rho}\right)\nabla\cdot q_s$	ρ: bulk density q_s: mass sediment transport rate per unit width
Mass transport rate of regolith, q_s	$q_s=-k\nabla\cdot z$	k: diffusion coefficient
Maximum stable bedrock hillslope height, H_c	$H_c=\frac{4C}{\rho g}\frac{\sin\beta\cos\phi}{[1-\cos(\beta-\phi)]}$	C: rock mass cohesion g: gravitational acceleration β: topographic slope ϕ: rock mass angle of internal friction
Stream power per unit bed width, Ω	$\Omega=\frac{\gamma APC_r S}{w}$	γ: flow unit weight A: contributing drainage area P: precipitation rate C_r: runoff coefficient S: channel bed slope w: flow width
Alluvial sediment mass transport rate, q_s	$q_s=k_a(\Omega-\Omega_0)$	k_a: empirical transport coefficient Ω_0: threshold stream power for channel initiation
Bedrock channel incision rate, $\partial z_b/\partial t$	$\frac{\partial z_b}{\partial t}=k_b\Omega_{excess}$	k_b: empirical incision coefficient Ω_{excess}: excess stream power z_b: elevation of bedrock channel

fluvial sediment transport and bedrock channel incision (Fig. 2; Table 1). Regolith transport is modelled as a linear diffusive process; Densmore *et al.* (1998) showed that this component of the model plays a minor role in the evolution of montane landscapes. Bedrock landsliding is modelled as a stochastic process modulated by rock mass strength, defined by rock cohesion and static angle of internal friction. Probability of landslide occurrence at any one point in the landscape is proportional to the height of the hillslope relative to the maximum stable hillslope height (Table 1). Landslide debris is routed down the path of steepest descent as a tongue of sediment and remains mobile as long as the surface slope exceeds 2°, which crudely simulates transport and deposition by debris flows. However, it is important to note that no attempt has been made to capture the composition, dynamics or rheological variability of real debris flows (e.g. Whipple & Dunne, 1992; Blair & McPherson, 1994).

The channel network is defined dynamically on the basis of the spatial distribution of a slope–drainage area product, with the threshold value for channel initiation chosen empirically (see Densmore *et al.*, 1998). Sediment delivered to the channel network by hillslope processes is transported at a rate that is directly proportional to stream power per unit bed width. Bedrock channel incision is allowed only if the stream power at a particular node exceeds the power required to transport all available sediment (Fig. 2; Table 1). Stream power itself is proportional to precipitation rate (Table 1). As the model operates over 10-yr time steps, precipitation rate as used by the model is in fact a very simplified proxy for a host of hydrological variables, including true mean annual precipitation rate, storm frequency and intensity, and evapotranspiration. It is important to realize that these diverse variables are grouped into a single parameter for convenience. We thus focus on relative, rather than absolute, variations in the precipitation rate parameter and do not employ real precipitation rate data from the Death Valley region.

Sediment that is transported to the boundaries of the model space is allowed to spill off the edge of the space, at which point it is lost from the model system. No baselevel constraints are applied to the boundaries. In the experiments described below, sediment is transported from the footwall to the hangingwall, where it fills the available volume created by vertical and horizontal tectonic displacements. Sediment that cannot be accommodated within the hangingwall is transported down across a system of hangingwall alluvial fans and spills off the model edge. This is equivalent to having an axial river at the downfan edge of the model space, although in reality an axial river would act as an independent baselevel control for the fan system; this is not simulated here. The model fans are not closed systems, in that sediment is allowed to escape from the model space. The magnitude of this leakage is measured by a fan efficiency factor (Whipple & Trayler, 1996; Allen & Hovius, 1998), defined as 0 for complete bypass of sediment out of the fan system and 1 for complete deposition of sediment on the fan surface. The fan efficiency factor in these experiments varies between 0.5 and 0.7. In sum, we emphasize that the geometry of the fan systems in these experiments is constrained solely by the hangingwall subsidence rate and by the position of the edges of the model space. Note that this introduces a maximum fan area, dictated

by the width of the hangingwall (5 km) and the spacing between adjacent footwall catchments ($\sim$1.5 km).

Densmore *et al*. (1998) described and calibrated the algorithms within *Zscape* and demonstrated that the development of realistic footwall topography associated with active normal faults required hillslope sediment transport by bedrock landslides. Their numerical experiments indicated that constant fault slip and precipitation rates eventually yielded landscapes in which rock uplift was balanced by denudation by landsliding and bedrock channel incision, giving rise to an invariant footwall morphology that was statistically similar to actively uplifting footwall landscapes in the Basin and Range province.

Ellis *et al*. (1999) showed that many of the characteristic landforms of the Basin and Range, such as triangular facets, concordant spurs, embayed mountain fronts and rangefront pediments, could be constructed by relatively simple perturbations to the basic model landscape. They observed that a Basin-and-Range-scale footwall block required $\sim 10^6$ yr to evolve from a flat initial landscape to a range with a steady value of relief. Once the morphology of the footwall block was established, variations in the slip rate on the bounding normal fault caused adjustments in relief over a time span of $\sim 10^5$ yr.

For the present study we have modified *Zscape* to explicitly track spatial variations in denudation (as measured by catchment-averaged erosion rates) and deposition (as measured by fan-averaged deposition rates). Details of the parameter values used in the numerical experiments presented here are given in Table 2.

EXPERIMENTS 1 & 2: FAN AND CATCHMENT AREAS

Perhaps the most fundamental property of catchment–fan systems is the ratio of fan area to catchment area (Bull, 1962, 1964; Hooke, 1968; Harvey, 1989; Lecce, 1991; Harvey, 1992; Whipple & Trayler, 1996; Allen & Hovius, 1998), termed ϕ by Allen & Hovius (1998). The widely accepted power law relationship between fan area and catchment area has been examined in a wide range of tectonic and climatic settings. Some authors (Oguchi & Ohmori, 1994; Milana & Ruzycki, 1999) attribute the relationship primarily to climatic setting, whereby increases in the water discharge from a catchment increase its efficiency at transporting sediment far from the fan apex. Others, including Whipple & Trayler (1996) and Allen & Hovius (1998), have proposed that ϕ is more influenced by the tectonic displacement rate at the fan apex. In this model, high fault slip rates drive base level fall and headward fluvial erosion within the catchment, extending the catchment and placing it in competition with its neighbours for drainage area. High slip rates also give rise to rapid development of accommodation; consequently, while the volume of fan material may be relatively high, plan-view fan areas are small. The net effect of catchment expansion (limited by range dimensions and competition with neighbouring catchments) and small fan areas should yield an inverse relationship between fault slip rate and ϕ.

Variations in fault slip rate may also explain the striking differences in catchment and fan morphology between the eastern and western sides of Death Valley (Fig. 3). Death Valley contains excellent and well-studied examples of both alluvial and debris-flow fans (e.g. Denny, 1965; Hooke, 1972; Blair, 1999a,b). The Quaternary slip rate on the dextral transtensional Death Valley–Furnace Creek fault that bounds the eastern margin of Death Valley is 3–6 mm yr^{-1} based on palaeoseismological data (Reheis & Sawyer, 1997) and geodetic observations (Bennett *et al*., 1997). This rate is an upper bound on the normal slip rate along the Black Mountains (Fig. 3). Despite poor data, there is consensus that fault slip rates and displacement along the front of the Black Mountains have far exceeded those along the front of the Panamint Range, on the western margin, over geological time (Butler *et al*., 1988; Brogan *et al*., 1991).The fans on either side of the valley contrast markedly, with extensive, coalesced fans adjacent to the Panamint Range and small, isolated fans adjacent to the Black Mountains (Fig. 3). Catchments in the Panamint Range are pear-shaped, with up to 3500 m of relief. Catchments in the Black Mountains are somewhat more elongate in plan view, and the relief is considerably less. Thus, values of ϕ are an order of magnitude higher on the western side than on the east (Fig. 4).

We evaluate the role of fault slip rate by examining the values of ϕ that arise in synthetic landscapes produced by normal dip slip at different rates, all else being equal. In experiment 1, footwall rock uplift is driven by dip slip along a normal fault with a mean slip rate of 0.5 mm yr^{-1}. The model precipitation rate is constant at 0.5 m yr^{-1}. The model is run until it reaches steady state, as defined by constant maximum footwall relief and an approximate balance between rock uplift and denudation everywhere within the model space; this occurs after a run time of $\sim$1000 kyr. The resulting landscape (Fig. 5) shows many of the characteristic land-

Table 2. Parameters used in numerical experiments.

Experiment	1	2	3	4	5
Fault slip rate (mm yr^{-1})	0.5	2.0	2.0–0.5	0.5	2.0–0.5
Model precipitation rate (m yr^{-1})	0.5	0.5	0.5	0–1.0	0–1.0
Fault dip (degrees)	45	45	45	45	45–70

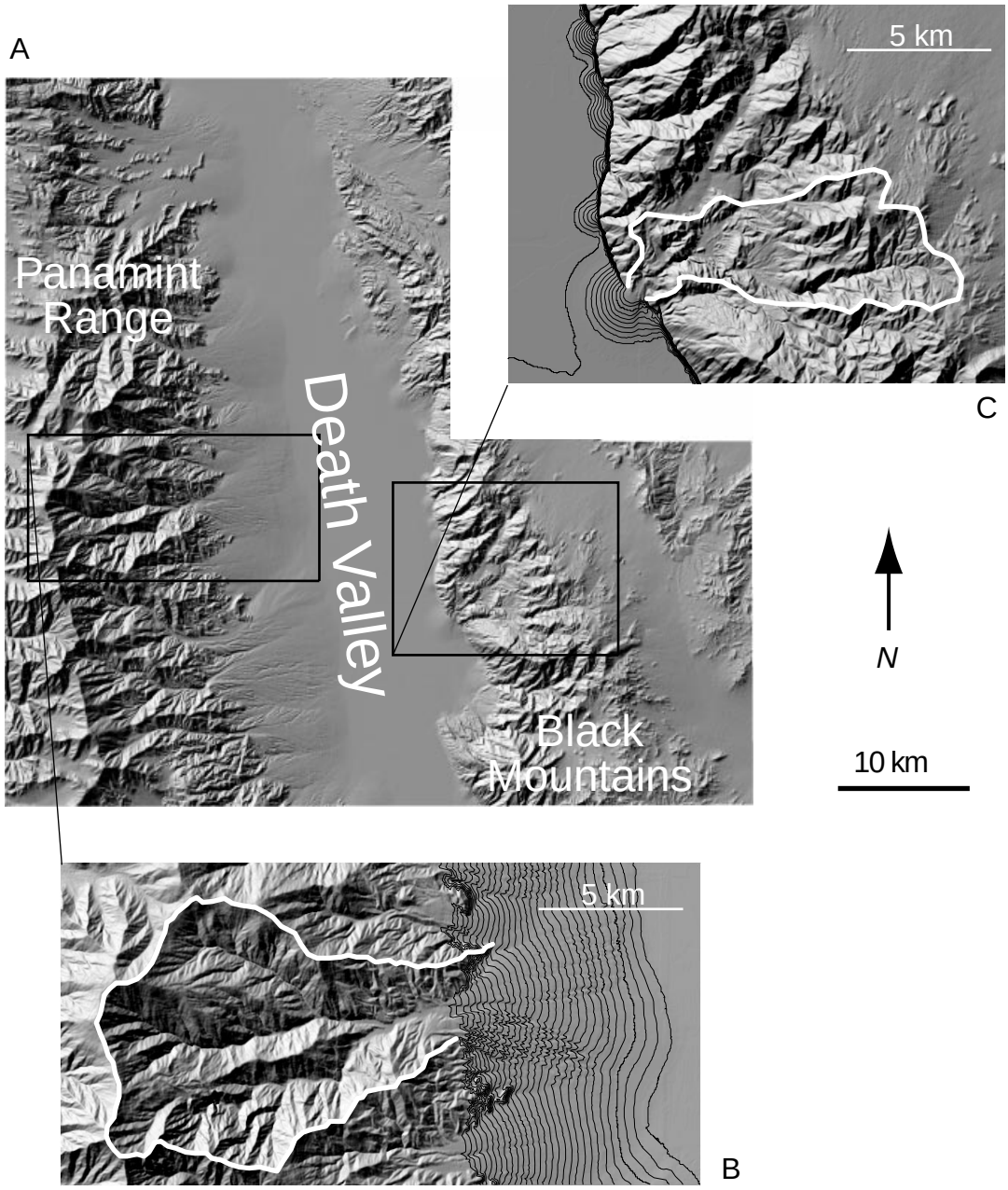

Fig. 3. A, shaded relief view of topography in the Death Valley region, south-eastern California. Data taken from USGS 30-m digital elevation models. B, close-up of Hanaupah Canyon catchment and fan, Panamint Range. Contour interval 20 m. Note pear-shaped catchment and large fan, partially coalesced into Panamint Range bajada. C, close-up of Copper Canyon catchment and fan, Black Mountains. Contour interval 10 m. Note elongate catchment and small, isolated fan.

forms associated with normal fault-bounded ranges, and is very similar to those discussed in Densmore *et al.* (1998) and Ellis *et al.* (1999). Of particular interest here are the well-developed catchment–fan systems that link the footwall and hangingwall. The ratios of fan to catchment areas in experiment 1 are scattered in the range $0.05 < \phi < 6.0$ (Fig. 6), similar to the range of ϕ-values observed in the Basin and Range (Allen & Hovius, 1998). The mean value of ϕ from experiment 1 is 2.20.

Experiment 2 is identical to experiment 1, except that the mean fault slip rate is 2.0 mm yr^{-1}. The landscape is allowed to evolve to steady state as above. While ϕ values from experiment 2 are scattered in a similar range to those from experiment 1, the higher slip rate in expt 2 yields, on average, lower values of ϕ (mean value 0.99), indicating smaller fans for a given catchment size (Fig. 6). Repeated runs with different model precipitation rates show that this small but systematic decrease in ϕ occurs for precipitation rates between 0.1 and 1.0 m yr^{-1}.

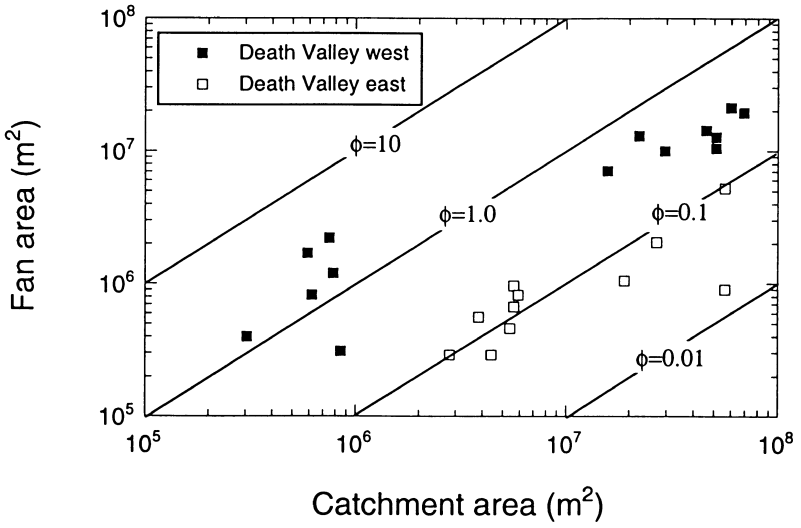

Fig. 4. Fan and catchment areas from the western, slowly deforming (filled symbols) and eastern, rapidly deforming (open symbols) margins of Death Valley. Data from Denny (1965). Each symbol represents a single catchment–fan pair. Also shown are lines of constant ϕ; note logarithmic axes.

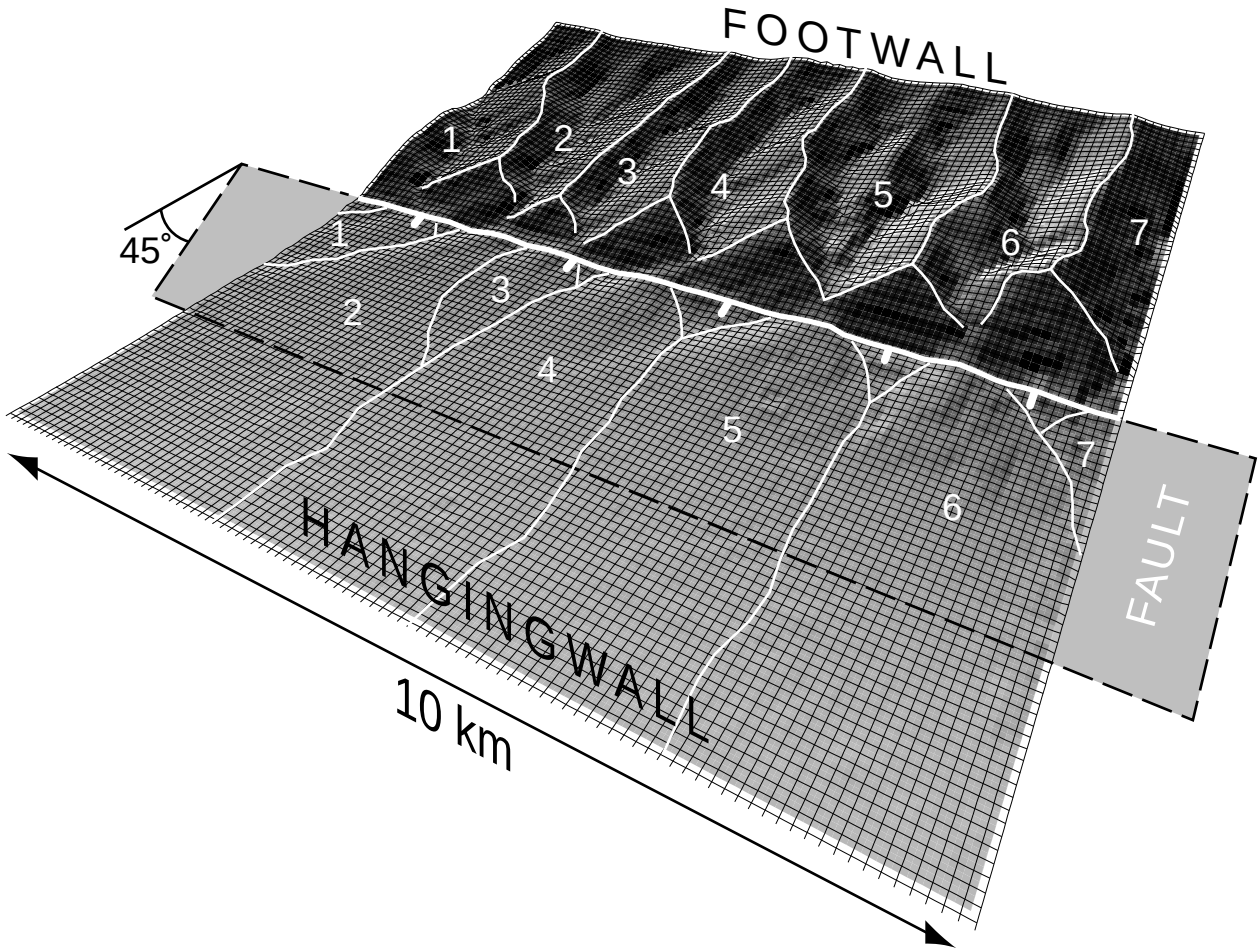

Fig. 5. Synthetic landscape developed at the end of experiment 1, after 1000 kyr of model run time. Slip on a single, 45°-dipping normal fault (shaded) yields a three-dimensional tectonic displacement field that is applied every 3400 yr, giving a long-term slip rate of 0.5 mm yr^{-1}. Model precipitation rate was constant at 0.5 m yr^{-1}. Note the elongate footwall catchments, separated by faceted spurs, and the coalesced fans or bajada that occupies the hangingwall. Individual catchment–fan pairs are denoted by numbers.

Much of the scatter seen in Fig. 6 is due to the fact that the geometry and sizes of the footwall catchments are highly variable in time, even in steady state, due to competition between catchments for the scarce resource of drainage area (Anderson *et al.*, 1999). Drainage area is captured by one catchment at the expense of another over time scales of $\leq$100s of kyr (Ellis *et al.*, 1999; Fig. 7), which leads to temporal variability in the loci of

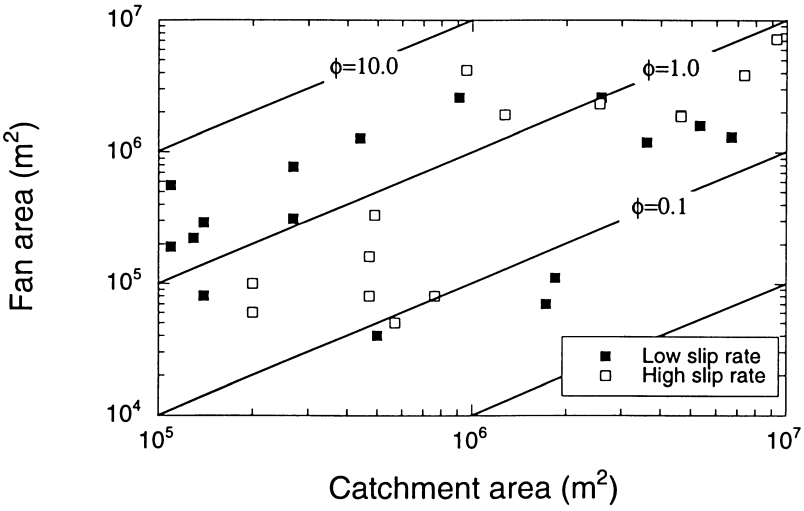

Fig. 6. Fan and catchment areas generated by experiments 1 and 2. Each symbol represents a single catchment–fan pair. Filled symbols show results from experiment 1, with mean fault slip rate of 0.5 mm yr^{-1}. Open symbols show results from experiment 2, with slip rate of 2.0 mm yr^{-1}. Model precipitation rate for both experiments was 0.5 m yr^{-1}. Compare with Fig. 4. Note strong scatter of data between $0.05 < \phi < 6.0$, consistent with Basin and Range catchment–fan systems (Allen & Hovius, 1998); however, on average, the higher slip rate during experiment 2 yields lower ϕ values (mean ϕ 2.20 from experiment 1, 0.99 from expt 2).

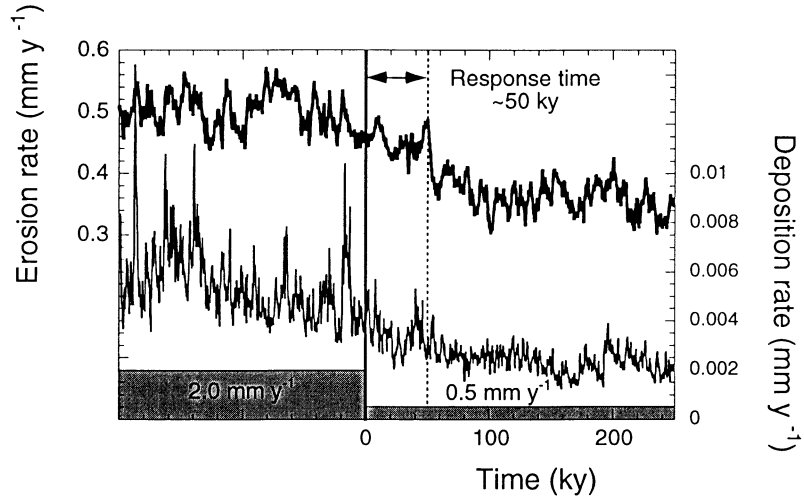

Fig. 7. Mean catchment-averaged erosion rate (heavy line) and mean fan deposition rate (thin line) before and after the fault slip rate decrease during experiment 3. Slip rate is shown by the grey bars, and the vertical line marks the slip rate decrease. Rates are calculated over 20 time steps, equivalent to 200 yr. Note the progressive decrease in erosion and deposition rates to new equilibrium values. The response times, defined as the time required for each rate to fall to 1/e of its initial value, are 56 kyr for erosion rate and 48 kyr for deposition rate. Mean fan deposition rate is several orders of magnitude lower than catchment erosion rates, reflecting (1) high ratios of fan to catchment area ($\phi > 1.0$) and (2) transport of sediment downfan and off the model space.

sediment discharge to the hangingwall. Thus at any one instant during an experiment, such as those represented by Fig. 6, there will exist catchment–fan systems that are not in equilibrium and do not show the expected power law area relationship. Examination of fan and catchment areas at other times during expts 1 and 2 yields different distributions of ϕ albeit with similar ranges and means.

EXPERIMENTS 3 & 4: RESPONSES TO TECTONIC AND CLIMATIC CHANGE

In the numerical experiments described by Densmore *et al.* (1998) and Ellis *et al.* (1999), imposition of a constant strain rate and a steady precipitation rate on an initially flat landscape eventually gave rise to a steady-state footwall topography, as defined by approximately constant mean catchment relief. The increase in relief with time could be fit by a function of the form $[1 - \exp(-t/\tau)]$, where the exponential decay time scale $\tau \sim 200$ kyr, essentially independent of the initial topographic form (Densmore *et al.*, 1998; Ellis *et al.*, 1999). This time scale thus represented the minimum time required to 'grow' footwall topography within a Basin-and-Range-scale crustal block, and can be interpreted as a characteristic 'response time' to significant changes in tectonic activity.

Here we evaluate the response of the coupled catchment–fan system to smaller, more realistic perturbations in tectonic and climatic boundary conditions, such as those associated with the transfer of slip to neighbouring faults during evolution of an extending region (e.g. Gupta *et al.*, 1998) or with orbitally forced variations in climate. Specifically, we examine changes in synthetic catchment–fan systems due to (1) changes in the slip rate on the bounding normal fault and (2) periodic variations in model precipitation rate.

Experiment 3: step change in fault slip rate

In experiment 3, an initial set of catchments and fans is allowed to develop as in experiments 1 and 2, with a fault slip rate of 2 mm yr^{-1} and a constant model precipi-

tation rate of 0.5 m yr^{-1}. The landscape is allowed to evolve to a steady-state footwall relief, which takes approximately 1000 kyr. At this point, tectonic flux of material into the footwall through rock uplift is approximately balanced by erosional flux out onto the hangingwall. The fault slip rate is then decreased to 0.5 mm yr^{-1}, simulating the transfer of strain accommodation to another fault segment (e.g. Hodges *et al.*, 1989). The response of the catchment–fan systems to this step decrease in fault activity can be seen by tracking the mean catchment-averaged erosion rate and the mean fan-averaged deposition rate during the experiment (Fig. 7). Before the decrease, both erosion and deposition rates vary rapidly about a mean value that is essentially constant with time (Fig. 7). These rapid variations arise from the fact that, in *Zscape* as in many montane landscapes, sediment is liberated from the footwall hillslopes and delivered to the catchment–fan systems primarily via bedrock landslides (Hovius *et al.*, 1997; Densmore *et al.*, 1998). These landslides are randomly distributed in space and time, and follow power-law magnitude–frequency distributions (e.g. Hovius *et al.*, 1997). Thus, even in the face of constant tectonic and climatic conditions, we expect – and observe – that hillslope sediment delivery to catchments and fluvial sediment transport onto fans should vary strongly on relatively short time scales.

After the slip rate decrease during experiment 3, erosion and deposition rates decay to new mean values. We define the response time τ for each rate as the time required for each rate to fall to $1/e$ or $\sim 37\%$ of its initial value. The erosion rate decrease is consistent with $\tau = 56$ kyr, while the deposition rate decrease yields $\tau = 48$ kyr (Fig. 7). These response times are unaffected by variations in precipitation rate in the range of 0.3–1.0 m yr^{-1}, implying that they are a robust feature of catchments at this scale (~ 5 km catchment length). Experiments in which the slip rate is increased from 0.5 to 2.0 mm yr^{-1} yield similar ~ 50-kyr response times, leading us to argue that this is a robust (though parameter-dependent) feature of the model. Note, too, that the ~ 50-kyr response time is shorter by a factor of 4 than the ~ 200-kyr response time of similar landscapes to complete starts or stops in fault activity described by Ellis *et al.* (1999). We infer that fluctuations in slip rate that occur on time scales of less than ~ 50 kyr, including those associated with displacement during individual earthquakes, are effectively 'filtered' by the catchment–fan system and should not be easily discernible as marked changes in sediment delivery in the stratigraphic record.

Sediment liberated from footwall catchments has two possible fates – either it is deposited on fans within the hangingwall, or it is transported downfan and off the downslope edge of the model space. The discharge of sediment from the model space is interesting, as it reflects the balance between input of sediment to the hangingwall and the subsidence rate. In addition, the magnitude of sediment discharge dictates the volume of material that is reworked and removed from the fan system into distal or axial drainage systems. Because these distal or axial rivers are commonly sand-prone depositional systems, the discharge from the model space has direct relevance to the prediction of down-fan reservoir quality in rift settings.

The discharge of sediment per unit width from the model space during the early stages of experiment 3 is quite unsteady, despite steady rates of fault slip and precipitation (Fig. 8). Some of this variability is due to the episodic delivery of sediment to the hangingwall, as described above. In addition, downfan sediment transport occurs episodically, i.e. sediment travels across the fan to the model edge in short jumps, rather than all at once.

After the decrease in fault slip rate, sediment discharge from the model space rises to a peak before decaying to a new equilibrium value (Fig. 8). This counterintuitive result arises because, in the immediate aftermath of the slip rate decrease, the footwall continues to denude at relatively high rates, whereas the subsidence rate decreases instantaneously to a new, constant value. The sediment entering the hangingwall can no longer be accommodated within the model space, and much of the sediment is transported downfan and lost from the system. After $1-2\tau$ as footwall erosion rates and sediment discharge from the footwall decay toward new equilibria, the sediment discharge likewise stabilizes. The

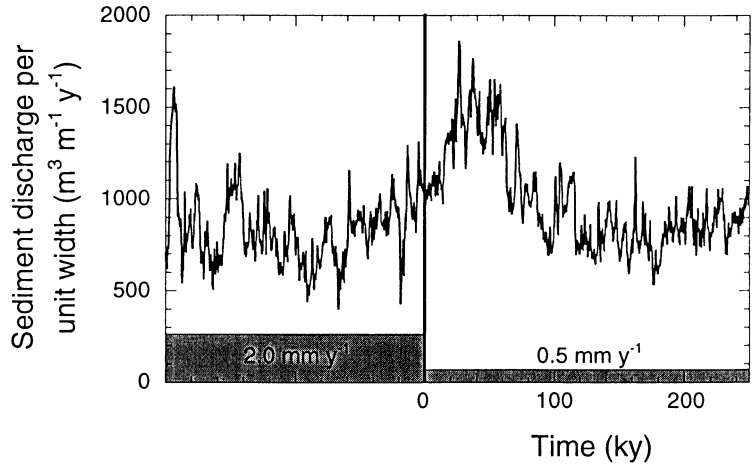

Fig. 8. Sediment discharge per unit width from the downfan edge of the model space before and after the fault slip rate decrease during experiment 3. The vertical line marks the slip rate decrease. Note oscillatory behaviour before the step change in fault slip rate, caused by episodic sediment delivery to and transport across the fan system. After the step change, sediment discharge from the model space briefly increases as hangingwall subsidence rates drop, then gradually decreases as footwall erosion rates decay.

transient nature of this sediment pulse is reflected by an abrupt, but short-lived, drop in the fan efficiency factor, indicating temporarily increased bypass of sediment out of the fans (Fig. 9). This phenomenon has strong implications for sediment storage and dispersal adjacent to dynamically evolving normal fault systems (e.g. Gupta *et al.*, 1998; Gupta *et al.*, 1999).

Experiment 4: periodic variation in precipitation rate

In experiment 4, an initial landscape is allowed to develop with a fault slip rate of 0.5 mm yr^{-1} and a constant model precipitation rate of 0.5 m yr^{-1}. Once approximate steady state has been reached, the model precipitation rate is allowed to vary sinusoidally between 0 and 1.0 m yr^{-1} with a period of 40 kyr (Fig. 10). This simulates, in a crude sense, the variation in precipitation between glacial and interglacial epochs. Experimental results are similar for precipitation rate variations with periods of 10–100 kyr.

In contrast to the delayed response of erosion and deposition rates to changes in slip rate observed in experiment 3, the landscape response to variations in precipitation rate is quite rapid (Fig. 10). During dry phases, the minimum in mean catchment erosion rate lags 4.5 kyr behind the minimum in precipitation rate; the mean fan deposition rate shows a similar lag of 2.7 kyr. During wet phases, both erosion and deposition rates reach peak values about 2.5 kyr before the peak in precipitation rate. These results imply that (1) sediment that accumulates on hillslopes and in catchments within the footwall during dry phases is rapidly mobilized and transported during the transition to wetter conditions, and (2) during wet phases the footwall is flushed of sediment, so that relatively little sediment remains in the catchments across multiple, closely spaced climate cycles.

Interestingly, peak deposition rates during wet phases decrease over the course of experiment 4. Tucker & Slingerland (1997) observed similar behaviour in numerical experiments of catchment response to sinusoidally varying runoff with a 1-kyr period, though not for variations with a 25-kyr period. They interpreted the decrease in peak deposition rate as evidence that phases

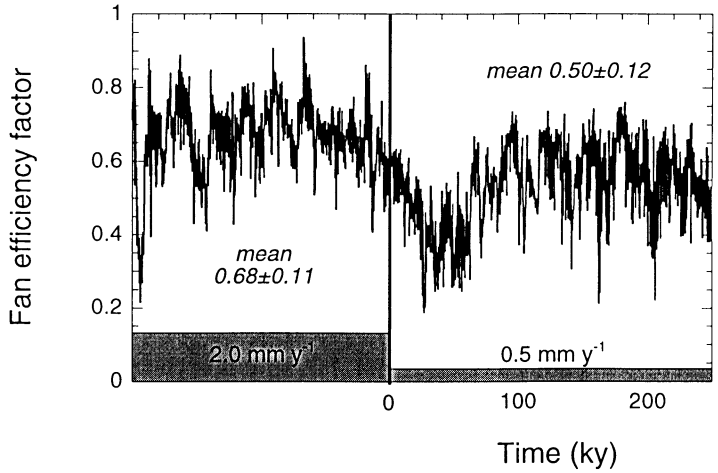

Fig. 9. Fan efficiency factor (Whipple & Trayler, 1996; Allen & Hovius, 1998) before and after the fault slip rate decrease during experiment 3. A fan efficiency factor of 0 indicates complete bypass of sediment out of the fan system, while 1 indicates complete deposition of sediment on the fan surface. The vertical line marks the slip rate decrease. Note the rapid decrease in fan efficiency immediately after the slip rate decrease due to the loss of hangingwall accommodation, indicative of an increase in the discharge of sediment bypassing the fan system. This effect persists for $\sim 10^5$ yr before footwall erosion rates drop sufficiently to achieve a new, quasi-equilibrium efficiency. The difference in mean efficiency factors before and after the slip rate decrease is highly significant (Student's *t*-test passed, $P < 0.001$).

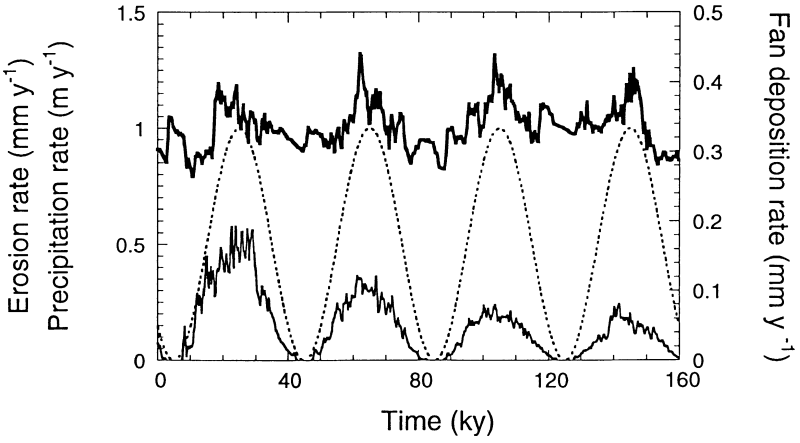

Fig. 10. Mean catchment-averaged erosion rate (heavy solid line) and mean fan deposition rate (light solid line) in the face of variable model precipitation rate during experiment 4. Model precipitation rate (dashed line) varies from 0 to 1.0 m yr^{-1} with a period of 40 kyr. Note the short (~ 2.5 kyr) offset between peak precipitation rates and peak erosion and deposition rates.

of high runoff denude the catchments of sediment so thoroughly that they do not 'heal' during subsequent dry phases, i.e. insufficient sediment accumulates during dry phases to allow constant rates of wet phase deposition. However, this cannot be the case in experiment 4, because if so we would expect that catchment erosion rates would decay as well; instead peak erosion rates are approximately constant during the experiment (Fig. 10).

Instead, we observe that the model fans prograde, and fan areas increase, during wet phases, but fan areas remain essentially static during dry phases. Sediment liberated from the footwall, which is approximately constant from one wet phase to another, is thus spread over a total fan area that grows progressively larger with time, giving rise to progressively lower mean fan deposition rates. This argument is supported by the time series of sediment discharge per unit width from the model space during experiment 4, which shows that sediment discharge varies directly in phase with precipitation rate, with little change in peak discharge values during the experiment (Fig. 11).

The rapid adjustments in erosion rate, in phase with variable precipitation rate, indicate that model catchments respond almost instantaneously to climatic changes. In these experiments, increased precipitation is expressed simply as increased stream power per unit bed width, thus increasing both sediment conveyance capacity and the rate of bedrock incision. No dynamic changes to other processes, such as weathering or denudation by landsliding, are incorporated. In reality, the transition to a wetter climate should trigger a complex response in the landscape due to increased vegetation cover, increased rates of weathering and hillslope sediment transport, and increased stream power, and changes to the flood hydrographs within individual catchments (e.g. Bull, 1991; Rinaldo *et al.*, 1995; Tucker & Slingerland, 1997). Our results therefore illustrate only one of the possible geomorphic effects of wet–dry cycles.

EXPERIMENT 5: FAN GEOMETRY AND PROGRADATION DISTANCE

The geometry of a basin margin fan, and in particular its progradation distance and stratigraphic expression, is the result of a balance between the temporal and spatial distribution of sediment discharge from the catchment and, importantly, the three-dimensional deformation field that creates space for sediment accumulation. This space is controlled by a variety of factors: coseismic and postseismic fault displacements, flexural and isostatic compensation of the sediment load, cooling following stretching of the underlying lithosphere, and lateral interactions between adjacent depositional systems. We focus here on the role of fault displacements in creating accommodation. The small width of most hangingwall basins in continental extensional settings, relative to the effective elastic thickness of the lithosphere, results in small differential flexural or isostatic displacements across the basin (e.g. Densmore *et al.*, 1998). Similarly, the short time scale of basin development and filling ($\sim$1–10 Myr; e.g. Smith, 1994) precludes significant thermal subsidence. We emphasize that horizontal fault displacements and vertical subsidence both play an important role in creating accommodation in extending regions.

While our experimental results are clearly dependent on the choice of parameters, we can place some constraints on the sufficient conditions for fan progradation to occur. Figure 12 summarizes the results of experiment 5, designed to evaluate the effects of fault slip rate, fault geometry and precipitation rate on fan progradation distance. Fan progradation for a single catchment–fan pair is defined by the maximum distance from the fault at which sediment from that catchment is deposited; its maximum value is 5 km, which is the distance between the fault and the downfan edge of the model space. Over short time scales ($< 10^4$ yr), fault geometry and slip rate have only weak effects on fan progradation distance. Development of small, discrete fans requires low precipitation rates (≤ 0.3 m yr^{-1}) and consequent low sediment discharge from the footwall block. Conversely, high precipitation rates (≥ 1.0 m yr^{-1}) yield high sediment discharge and rapidly prograding fans that coalesce into a bajada and extend to the downfan edge of the model space. Once again climatic variability dominates fault slip rate variability in determining the short-term morphology of the catchment–fan system.

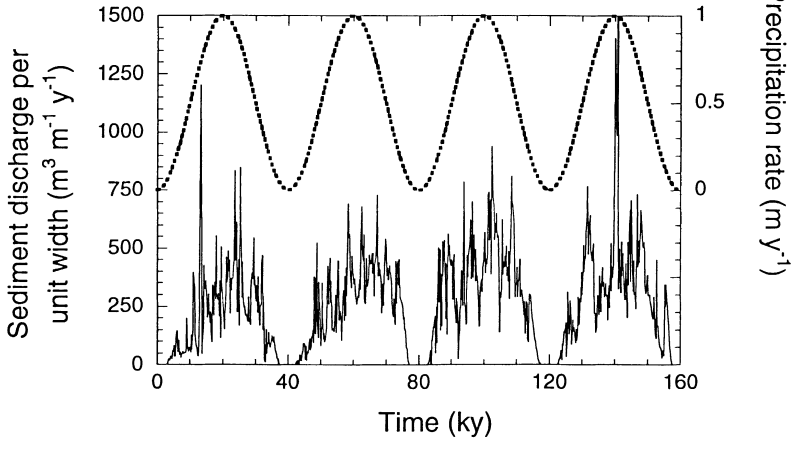

Fig. 11. Sediment discharge per unit width from the model space during experiment 4 (solid line) and model precipitation rate (dashed line). Discharge is in phase with precipitation rate, and peak values do not change appreciably through the experiment.

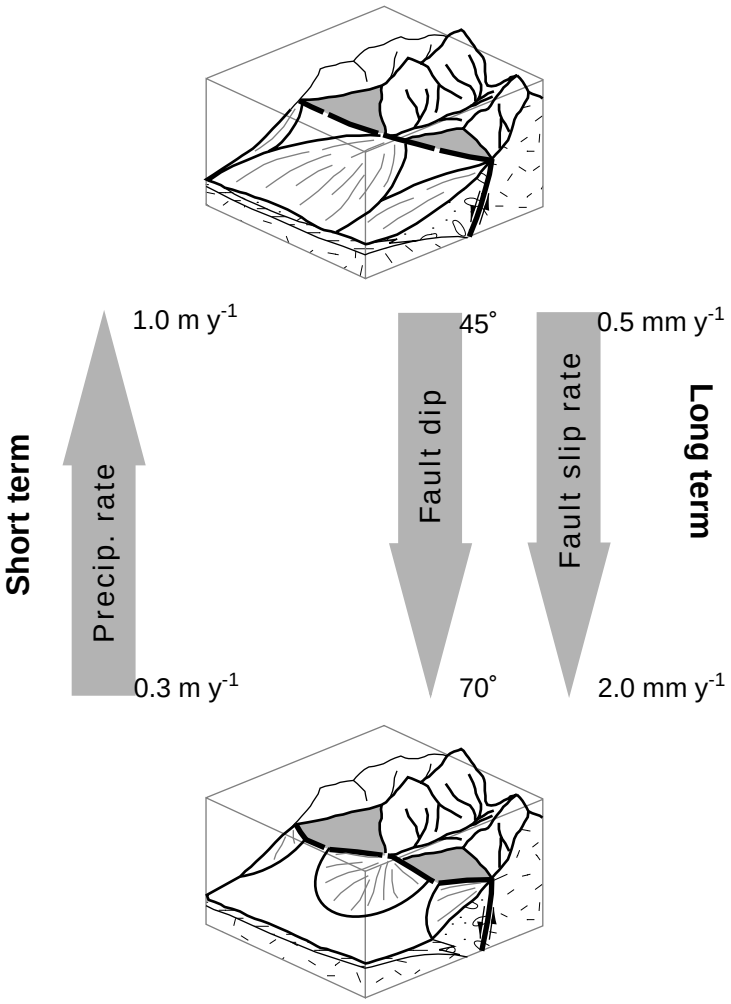

Fig. 12. Summary of sufficient conditions for fan progradation (expt 5). The upper diagram shows prograding, coalesced fans; the lower diagram shows nonprograding, isolated fans. Large arrows show the parameters evaluated and the values that always yield prograding or nonprograding fans. At short time scales ($<10^4$ yr), fan progradation is controlled by precipitation rate for most values of slip rate and fault dip. At longer time scales ($>10^4$ yr), fault geometry and slip rate become dominant for most values of precipitation rate.

At longer time scales, fan morphology in our experiments is dominated by tectonic controls for reasonable values of precipitation rate (0.25–1.0 m yr^{-1}). Low fault slip rates ($\leq$0.5 mm yr^{-1}) do not create enough accommodation to allow the formation of discrete fans; as a result, the hangingwall basin fills with sediment in the form of coalesced fans that extend to the downfan edge of the model space. High slip rates ($\geq$2.0 mm yr^{-1}) create sufficient volume to accommodate even high sediment discharge, resulting in discrete, nonprograding fans. Fault geometry influences fan progradation by setting the width of the fault displacement field and thus the volume of the hangingwall basin. Steeply dipping faults produce hangingwall basins with depocentres that are localized close to the fault trace (Fig. 12), while shallow fault dips give rise to a broader, shallower basin geometry. With intermediate fault slip (0.5 mm yr^{-1}) and precipitation (0.5 m yr^{-1}) rates, we find that fan progradation occurs at fault dips of $\leq 45^\circ$, but not at dips of $\geq 70^\circ$ (Fig. 12). In these respects, our results are consistent with the fan progradation model of Gordon & Heller (1993), in which subsidence rate is the dominant control on gravel progradation. Clearly, feedback and interplay between the parameters considered here, as well as the effects of other parameters (bedrock erodibility, runoff, vegetative cover, thermal and flexural subsidence), will complicate these simple relationships.

DISCUSSION

The results of our numerical experiments indicate that established catchment–fan systems associated with uplifting, Basin-and-Range-scale crustal fault blocks require approximately $\sim$50 kyr to adjust to perturbations in fault slip rate. Thus, rapid short-term variations in fault slip or slip rate, due for example to a single large earthquake, or to the spatial and temporal clustering observed in earthquakes in the Basin and Range province (Wallace, 1987), should not be easily discernible as a sediment pulse in the gross sedimentary architecture of the fan or down-fan systems. In essence, the catchment–fan system acts as a low-pass filter that effectively blurs high-frequency variations in fault activity.

Conversely, catchment–fan systems adjust rapidly to changes in precipitation rate because those changes are spatially widespread and simultaneously affect much or all of the system. We thus infer that the sedimentary record should record precipitation-induced changes in sediment flux from a catchment more faithfully than

those produced by changes in fault activity, and that observed short-term variability in the thickness and runout distances of fan deposits are much more likely to be due to climatic changes (e.g. Smith, 1994).

The persistence of a characteristic response time of 50 kyr for the adjustment of catchment–fan systems to tectonic boundary conditions suggests that we may define an effective system diffusivity, κ:

$$\kappa = L^2/\tau \quad (1)$$

where L is a characteristic length scale associated with the catchment–fan system and τ is the system response time. Given that the systems in our numerical experiments have $L \sim 10$ km and $\tau \sim 50$ kyr, we calculate an effective diffusivity of approximately 2000 $m^2\,yr^{-1}$.

It is clearly of interest to be able to gauge the response time of sediment routing systems with length scales longer than the 10-km scale investigated here. To do so requires an approximate knowledge of the effective diffusivities of such systems. This is a complex problem, partly because sediment routing systems contain varying proportions of geomorphological subsystems. For example, alluvial systems dominated by perennial rivers in large floodplains are likely to have different effective diffusivities to catchment–fan systems dominated by hillslope erosion and bedrock incision. In fact, if we accept that there is a good physical basis for treating river systems as diffusive entities (Paola *et al.*, 1992), there must be an increase in the effective diffusivities of fluvial systems compared to basin margin fans in order to explain their lower gradients.

Dade & Friend (1998) estimated effective diffusivities and response times of a selection of present-day rivers by considering the time required for a channel to achieve a 'graded' or 'equilibrium' profile along its entire length following a perturbation. The effective diffusivities of the rivers selected by Dade & Friend (1998; Table 2) were calculated using the water discharge per unit width and a relative sediment mobility parameter that incorporated the effects of both bedload and suspended load transport. Estimated effective diffusivities by this method are $10^8\,m^2\,yr^{-1}$ and $5 \times 10^8\,m^2\,yr^{-1}$ for the Brahmaputra and Indus rivers, respectively, corresponding to channel response times of 85 and 21 kyr. However, these values do not reflect the large buffering effect of extensive floodplain systems. Métivier & Gaudemer (1999) estimated the diffusivities of large Asian channel–floodplain systems by relating the sediment discharge at the river mouth to the width and mean slope of the system:

$$\kappa = \frac{Q_s}{w\left\langle \frac{\partial z}{\partial x} \right\rangle} \quad (2)$$

where Q_s is the mass transport rate ($m^3\,yr^{-1}$), w is the floodplain width and $\langle \partial z/\partial x \rangle$ is the spatially averaged topographic slope, taken as the elevation change between the upstream and downstream ends of the floodplain divided by its length. Data provided by Métivier & Gaudemer (1999; Table 3) yield effective floodplain diffusivities in the range of 10^6–$10^7\,m^2\,yr^{-1}$. These values are equivalent to response times of 10^5–10^6 yr for large Asian river floodplains, such as the Brahmaputra and Indus. Métivier & Gaudemer (1999) consequently suggested that the good correlation between present-day solid fluxes in Asian rivers and time-averaged deposition rates over the last 2 Myr derived from the stratigraphy of marine depocentres (Métivier *et al.*, 1999) may be explained by the strong buffering action of large floodplains on short-term variations in hillslope sediment fluxes.

In our experiments, $Q_s \sim 2 \times 10^4\,m^3\,yr^{-1}$, $w \sim 100$ m and $\langle \partial z/\partial x \rangle \sim 0.1$, giving an alternative effective diffusivity of $\sim 2000\,m^2\,yr^{-1}$ – very similar to the diffusivity estimated on the basis of response time, but several orders of magnitude smaller than the much larger, but less steep, Asian floodplains. We propose that, in the relatively confined sediment routing systems of continental rifts, effective diffusivities are likely to be intermediate between those of catchment–fan systems typical of the Basin and Range, and those of large fluvial systems. This dependence of effective diffusivity on system scale and dominant geomorphic process has been widely used in models of landscape and foreland basin evolution (e.g. Flemings & Jordan, 1989; Kooi & Beaumont, 1994; Tucker & Slingerland, 1996). Taking an effective diffusivity for a rift sediment routing system of 10^4–$10^5\,m^3\,yr^{-1}$, response times for length scales an order of magnitude larger (10^2 km) than those investigated here will be in the range of 10^5–10^6 yr. This illustrates the trade-off between the high diffusivities and large size of fluvial-dominated channel–floodplain systems, and the lower diffusivities and smaller size of hillslope-dominated catchment–fan systems.

Geomorphic studies inevitably emphasize the role of climate on fan dimensions and profiles (e.g. Lustig, 1965; Nemec & Postma, 1993; Ritter *et al.*, 1995), whereas investigations geared to geological time scales focus on the overriding influence of tectonics through its control on footwall uplift and accommodation in the hangingwall. Part of the resolution of this paradox may be that the entire fan surface is rarely simultaneously active during a sediment transport event. Consequently, the ratio of total fan area to catchment area is representative of the integration over time of a large number of sediment transport events that encompass the entire fan, and therefore scales on tectonic parameters that set the accommodation required for long-term fan preservation. On the other hand, the sediment volumes, runout distances, and surface profiles resulting from individual flood events, or events clustered within a high-frequency climatic interval, are more likely to scale on their triggering climatic mechanisms.

The influence of tectonics may also be veiled by the fact that assessment of fault slip rate, let alone temporal variations in slip rate, in the semi-arid and arid regions

in which catchment–fan systems are best expressed is problematical. In addition, our numerical model results highlight important unforced variability in sediment discharge due to (1) spatially and temporally stochastic delivery of sediment to channels, and (2) competition between footwall catchments for the scarce resource of drainage area. We suggest that, while recent faulting may be locally important in changing base level, and incrementally important in controlling hangingwall subsidence and footwall rock uplift, its effects are likely to be strongly overprinted by climatic events over the short observational time scales characteristic of geomorphic studies. High-frequency sedimentological variations observed within a fan record away from the immediate vicinity of fault scarps are likely to be dominated by changes in climate. However, longer term cyclicity in the stratigraphy of fan and down-fan depositional systems may indeed reflect changes in tectonic boundary conditions, and thus require a knowledge of the history of fault slip rate over time.

There is therefore a dichotomy of perspective between the geomorphological and geological aspects of catchment–fan systems. What is increasingly required is an analysis of the stratigraphy of fan deposits at a range of time scales to reveal the dominant frequencies of depositional cycles, which will necessitate the best possible stratigraphic chronologies.

CONCLUSIONS

The results of our numerical experiments into the dynamics of catchment–fan systems on uplifting, Basin-and-Range-scale fault blocks can be summarized as follows:

1 The ratio of fan area to catchment area, ϕ, is an integrated signal reflecting slip rate on the range-bounding fault. High slip rates give rise to catchment–fan systems with low values of ϕ, and *vice versa*, though there is considerable scatter in our experimental data.

2 Established catchment–fan systems with length scales of ~ 10 km respond to changes in fault slip rate only after a response time of $\tau \sim 50$ kyr, regardless of climatic conditions. This corresponds to a system-scale effective diffusivity of approximately 2000 $m^2\,yr^{-1}$, and implies that slip rate variations on time scales of < 50 kyr are unlikely to be diagnosed from the stratigraphic record.

3 After a decrease in fault slip rate, sediment discharge from a catchment–fan system into distal or axial depositional environments initially rises due to a decrease in hangingwall accommodation. The discharge then decays to a new equilibrium value over $1-2\tau$ as the footwall is denuded.

4 Catchment–fan systems are in phase with variations in model precipitation rate, with response times of < 5 kyr.

5 Away from the immediate vicinity of the fault scarp, high-frequency (period < 50 kyr) variations in stratigraphic records of fan deposition are most likely to reflect rapid changes in climatic conditions. Changes in tectonic boundary conditions are more likely to be recorded by longer-term (period ≥ 50 kyr) stratigraphic cycles.

ACKNOWLEDGMENTS

Zscape was developed under a grant from the NASA Topography and Surface Change Program to Robert Anderson and Michael Ellis. We thank Michael Ellis and Alastair Ruffell for discussions. Greg Tucker, Gary Smith and Sanjeev Gupta provided helpful and constructive reviews.

REFERENCES

Allen, P.A. & Hovius, N. (1998) Sediment supply from landslide-dominated catchments: implications for basin-margin fans. *Basin Res.*, **10,** 19–35.

Anderson, R.S., Densmore, A.L. & Ellis, M.A. (1999) The generation and degradation of marine terraces. *Basin Res.*, **11,** 7–19.

Bennett, R.A., Wernicke, B.P., Davis, J.L., Elósegui, P., Snow, J.K., Abolins, M.J., House, M.A., Stirewalt, G.L. & Ferrill, D.A. (1997) Global Positioning System constraints on fault slip rates in the Death Valley region, California and Nevada. *Geophys Res. Letters*, **24,** 3073–3076.

Blair, T.C. (1999a) Sedimentology of the debris-flow-dominated Warm Spring Canyon alluvial fan, Death Valley, California. *Sedimentology*, **46,** 941–965.

Blair, T.C. (1999b) Sedimentary processes and facies of the waterlaid Anvil Spring Canyon alluvial fan, Death Valley, California. *Sedimentology*, **46,** 913–940.

Blair, T.C. & McPherson, J.G. (1994) Alluvial fan processes and forms. In: *Geomorphology of Desert Environments* (Ed. by A.D. Abrahams & A.J. Parsons), pp. 354–402. Chapman & Hall, London.

Brogan, G.D., Kellogg, K.S., Slemmons, D.B. & Terhune, C.L. (1991) Late Quaternary faulting along the Death Valley-Furnace Creek fault system, California and Nevada. *U.S Geol. Surv. Bull.*, **1991**.

Bull., W.B. (1962) Relations of alluvial fan size and slope to drainage basin size and lithology in western Fresno County, California. *U.S. Geol. Surv. Prof. Pap.*, **450-B,** 51–53.

Bull., W.B. (1964) Geomorphology of segmented alluvial fans in western Fresno County, California. *U.S. Geological Survey Professional Paper*, **352-E,** 89–129.

Bull., W.B. (1991) *Geomorphic Responses to Climatic Change*. Oxford University Press, New York.

Butler, P.R., Troxel, B.W. & Verosub, K.L. (1988) Late Cenozoic history and styles of deformation along the southern Death Valley fault zone, California. *Geol. Soc. Am. Bull.*, **100,** 402–410.

Dade, W.B. & Friend, P.F. (1998) Grain size, sediment transport regime and channel slope in alluvial rivers. *J. Geol.*, **106,** 661–675.

Denny, C.S. (1965) Alluvial fans in the Death Valley region, California and Nevada. *U.S. Geol. Surv. Prof. Pap.*, **466,** 1–62.

Densmore, A.L., Ellis, M.A. & Anderson, R.S. (1998) Landsliding and the evolution of normal fault-bounded mountain ranges. *J. Geophys. Res.*, **103,** 15203–15219.

Dixon, T.H., Robaudo, S., Lee, J. & Reheis, M.C. (1995)

Constraints on present-day Basin and Range deformation from space geodesy. *Tectonics*, **14,** 755–772.

Ellis, M.A., Densmore, A.L. & Anderson, R.S. (1999) Development of mountainous topography in the Basin Ranges, U.S.A. *Basin Res.*, **11,** 21–41.

Flemings, P.B. & Jordan, T.E. (1989) A synthetic stratigraphic model of foreland basin development. *J. Geophys. Res.*, **94,** 3851–3866.

Gordon, I. & Heller, P.L. (1993) Evaluating major controls on basinal stratigraphy, Pine Valley, Nevada: Implications for syntectonic deposition. *Geol. Soc. Am. Bull.*, **105,** 47–55.

Gupta, S., Cowie, P.A., Dawers, N.H. & Underhill, J.R. (1998) A mechanism to explain rift-basin subsidence and stratigraphic patterns through fault-array evolution. *Geology*, **26,** 595–598.

Gupta, S., Underhill, J.R., Sharp, I.R. & Gawthorpe, R.L. (1999) Role of fault interactions in controlling synrift sediment dispersal patterns: Miocene, Abu Alaqa Group, Suez Rift, Sinai, Egypt. *Basin Res.*, **11,** 167–189.

Harvey, A.M. (1989) The occurrence and role of arid-region alluvial fans. In: *Arid Region Geomorphology* (Ed. by D.S. Thomas), pp. 136–158. Belhaven Press, London.

Harvey, A.M. (1992) Controls on sedimentary style on alluvial fans. In: *Dynamics of Gravel-Bed Rivers* (Ed. by P. Billi, R.D. Hey, C. R. Thorne & P. Taconi), pp. 518–534. Wiley, Chichester, UK.

Hodges, K.V., McKenna, L.W., Stock, J., Knapp, J., Page, L., Sternlof, K., Silverberg, D., Wüst, G. & Walker, J.D. (1989) Evolution of extensional basins and Basin and Range topography west of Death Valley, California. *Tectonics*, **8,** 453–467.

Hooke, R.L. (1968) Steady-state relationships on arid region alluvial fans in closed basins. *Am. J. Sci.*, **266,** 609–629.

Hooke, R.L. (1972) Geomorphic evidence for late Wisconsin and Holocene tectonic deformation, Death Valley, California. *Geol. Soc. Am. Bull.*, **83,** 2073–2098.

Hovius, N., Stark, C.P. & Allen, P.A. (1997) Sediment flux from a mountain belt derived by landslide mapping. *Geology*, **25,** 231–234.

Kooi, H. & Beaumont, C. (1994) Escarpment evolution on high-elevation rifted margins: insights derived from a surface processes model that combines diffusion, advection, and reaction. *J. Geophys. Res.*, **99,** 12191–12209.

Lecce, S.A. (1991) Influence of lithological erosibility on alluvial fan area, western White Mountains, California and Nevada. *Earth Surf. Process. Landforms*, **16,** 11–18.

Lustig, L.K. (1965) Clastic sedimentation in Deep Springs Valley, California. *U.S. Geol. Surv. Prof. Pap.*, **352-F.**

Métivier, F. & Gaudemer, Y. (1999) Stability of output fluxes of large rivers in South and East Asia during the last 2 million years: implications on floodplain processes. *Basin Res.*, **11,** 293–303.

Métivier, F., Gaudemer, Y., Tapponier, P. & Klein, M. (1999) Mass accumulation rates in Asia during the Cenozoic. *Geophys. J. Int.*, **137,** 280–318.

Milana, J.P. & Ruzycki, L. (1999) Alluvial-fan slope as a function of sediment transport efficiency. *J. Sedim. Res.*, **69,** 553–562.

Nemec, W. & Postma, G. (1993) Quaternary alluvial fans in southwestern Crete; sedimentation processes and geomorphic evolution. In: *Alluvial Sedimentation* (Ed. by M. Marzo & C. Puigdefabregas), *Spec. Publ., Int. Ass. Sedimentol.*, **17,** 235–276.

Oguchi, T. & Ohmori, H. (1994) Analysis of relationships among alluvial fan area, source basin area, basin slope, and sediment yield. *Z. Geomorphol. Neue Folge,* **38,** 405–420.

Paola, C., Heller, P.L. & Angevine, C.L. (1992) The large scale dynamics of grain size variation in alluvial basins, 1: Theory. *Basin Res.*, **4,** 73–90.

Reheis, M.C. & Sawyer, T.L. (1997) Late Cenozoic history and slip rates of the Fish Lake Valley, Emigrant Peak, and Deep Springs fault zones. *Geol. Soc. Am. Bull.*, **109,** 280–299.

Rinaldo, A., Dietrich, W.E., Rigon, R., Vogel, G. & Rodriguez-Iturbe, I. (1995) Geomorphological signatures of varying climate. *Nature*, **374,** 632–634.

Ritter, J.B., Miller, J.R., Enzel, Y. & Wells, S.G. (1995) Reconciling the roles of tectonism and climate in Quaternary alluvial fan evolution. *Geology*, **23,** 245–248.

Smith, G.A. (1994) Climatic influences on continental deposition during late-stage filling of an extensional basin, southeastern Arizona. *Geol. Soc. Am. Bull.*, **106,** 1212–1228.

Tucker, G.E. & Slingerland, R.L. (1996) Predicting sediment flux from fold and thrust belts. *Basin Res.*, **8,** 329–349.

Tucker, G.E. & Slingerland, R.L. (1997) Drainage basin responses to climate change. *Water Resour. Res.*, **33,** 2031–2047.

Wallace, R.E. (1987) Grouping and migration of surface faulting and variations of slip rate on faults in the Great Basin province. *Seismol. Soc. Am. Bull.*, **77,** 868–876.

Whipple, K.X. & Dunne, T. (1992) The influence of debris-flow rheology on fan morphology, Owens Valley, California. *Geol. Soc. Am. Bull.*, **104,** 887–900.

Whipple, K.X. & Trayler, C.R. (1996) Tectonic control on fan size: the importance of spatially-variable subsidence rates. *Basin Res.*, **8,** 351–366.

Received 16 February 2000; revision accepted 5 October 2000.

